Polymer Journal (2016) 48, 481–486

www.nature.com/pj

ORIGINAL ARTICLE

Control over electrically bistable properties of layer-by-layer-assembled polymer/organometal multilayers

Sanghyuk Cheong[1,3], Younghoon Kim[1,3], Sook Won Ryu[2] and Jinhan Cho[1]

We demonstrate that nonvolatile memory devices can be prepared using electrostatic layer-by-layer (LbL)-assembled nanocomposite films, and additionally that their performance can be easily enhanced by an additional insertion of charge trap elements within the films. For this study, cationic poly(allylamine hydrochloride) (PAH) and anionic titania precursors (titanium (IV) bis(ammonium lactato) dihydroxide, TALH) were used for the preparation of electrostatic LbL-assembled nanocomposite films on a Pt-coated silicon wafer. The formed multilayer nanocomposites were converted into the transition metal oxide films (that is, TiO_x nanocomposites) after thermal annealing at 450 °C, and then, the top electrodes were deposited onto the TiO_x films to complete the device fabrication. When external bias was applied to the devices, these TiO_x-based devices displayed bipolar resistive switching property with an ON/OFF current ratio of ~ 10. However, the insertion of anionic graphene oxide (GO) nanosheets into the PAH/TALH multilayers produced GO-incorporated TiO_x films after thermal annealing, which exhibited memory performance with a high ON/OFF current ratio of ~ 10^4. Furthermore, we demonstrate that the switching mechanism of GO-incorporated TiO_x devices can be explained by the charge trap model.
Polymer Journal (2016) **48,** 481–486; doi:10.1038/pj.2016.4; published online 3 February 2016

INTRODUCTION

Nonvolatile memory devices such as charge trap flash, phase change, ferroelectric and resistive switching nonvolatile memory (RSNM) devices have attracted considerable attention due to the rapid expansion and evolution of mobile electronics.[1–12] Particularly, RSNM devices based on resistive switching materials that exhibit good memory performance, such as high ON/OFF current ratio $>10^2$, fast switching speed and low operating voltage with a simple device structure, have been recognized as being among the most promising candidates in a variety of next-generation nonvolatile memory devices.[6–8] In general, binary transition metal oxides (TMOs) (that is, TiO_x, NiO or ZrO_x or $SrTiO_3$) prepared through a vacuum deposition process have been used as resistive switching-active materials and have demonstrated a significant change in resistance states under applied voltage sweep. Recently, many efforts have been made to modify the electrical properties or improve the memory performance of RSNM devices through the insertion of additional electrically active components such as Au, Pt, Gd or IrO_2 within TMO layers.[13–16] Furthermore, the simple solution process rather than the vacuum process is needed for the preparation of low-cost and large-area RSNM devices. In connection with such a necessity, it has been reported that a variety of resistive switching-active films for high-performance RSNM devices can be prepared from the spin-coating of polymers containing charge trap elements (that is, graphene oxide (GO), carbon nanotube, metal nanoparticles and so on); in addition, the presence and uniformity of such charge trap sites have a significant effect on ON/OFF current ratio and device stability.[17–19] Although the deposition of an electrically active nanocomposite layer through a facile solution process such as spin-coating has an advantage in terms of easily preparing the RSNM devices, the devices prepared from such an approach still have much difficulty in securing high memory performance and long-term electric stability comparable to those of TMO-based devices. For example, if the charge trap elements such as inorganic nanoparticles are simply blended with the polymer binders without serious consideration of their reciprocal interactions, the spin-coating approach causes aggregates with dimensions of several hundreds of nanometers due to thermodynamically unfavorable interactions.[20] It should also be noted that aggregation or segregation phenomena have a detrimental effect on the memory performance of RSNM devices. Therefore, one of the most challengeable attempts in the field of RSNM devices is the development and design of resistive switching nanocomposite films with excellent memory performance, allowing a nanoscale-blending structure via a solution process.

Among the various deposition methods, it has been demonstrated that the layer-by-layer (LbL) assembly method based on a

[1]Department of Chemical and Biological Engineering, Korea University, Seoul, Republic of Korea and [2]Department of Laboratory Medicine, Kangwon National University School of Medicine Kangwondaehak-gil, Gangwon-do, Republic of Korea
[3]These authors contributed equally to this work.
Correspondence: Professor J Cho, Department of Chemical and Biological Engineering, Korea University, Anam-dong, Seongbuk-gu, Seoul 136-713, Republic of Korea.
E-mail: jinhan71@korea.ac.kr
or Professor SW Ryu, Department of Laboratory Medicine, Kangwon National University School of Medicine Kangwondaehak-gil, Chuncheon-si, Gangwon-do 200-701, Republic of Korea.
E-mail: ryusw@kangwon.ac.kr
Received 15 November 2015; revised 28 December 2015; accepted 4 January 2016; published online 3 February 2016

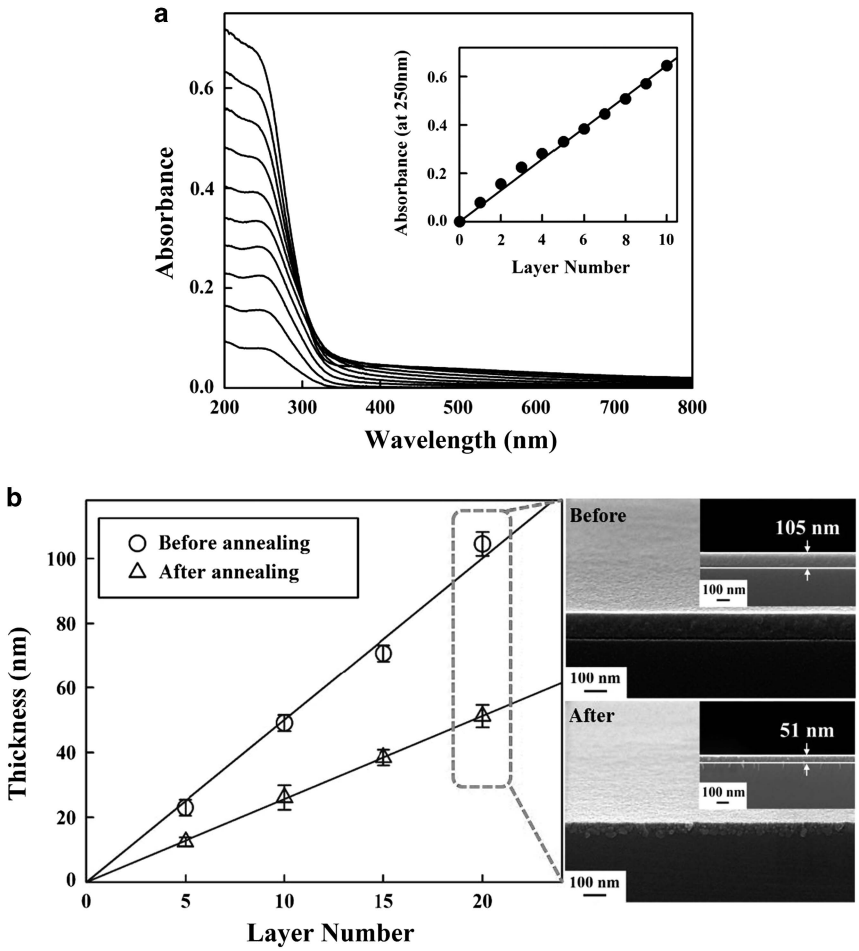

Figure 1 (**a**) UV–Vis spectra of $(PAH/TALH)_n$ multilayers measured with increasing the bilayer number (n). The inset of **a** shows the absorbance of TALH measured at 250 nm as a function of bilayer number. (**b**) Film thicknesses and s.e.m. images of (PAH and $TALH)_n$ multilayers before and after thermal treatment at 450 °C for 6 h (that is, 2 h under nitrogen and 4 h under oxygen). UV–Vis, ultraviolet–visible. A full color version of this figure is available at *Polymer Journal* online.

solution dipping, spin-coating or spray process is quite useful for preparing organic and/or inorganic nanocomposite films with tailored thickness, composition and functionalities on substrates of different sizes and shapes.[21–26] This approach is achieved by tuning the complementary interactions (that is, electrostatic, hydrogen-bonding or covalent interaction). In addition, the LbL assembly technique allows the electrical properties of nanocomposite film devices to be adjusted through a facile insertion of various functional components within films.[27] Therefore, our motivation was to fabricate the high-performance RSNM devices using LbL assembly. A main aim was to improve the memory performance (particularly, ON/OFF current ratio and performance stability) of nanocomposite films through the use of electrostatically charged inorganic precursor and charge trap elements, allowing electrostatic LbL assembly.

Herein, we introduce an LbL-assembled RSNM device with voltage-polarity-dependent bipolar switching behavior, high ON/OFF current ratio $>10^4$ and long-term stability. In addition, we demonstrate that the memory performance of nanocomposite films is significantly enhanced by the additional insertion of charge trap elements within TMO matrices. First, for this study, the nanocomposite films composed of anionic GO sheet, cationic poly(allylamine hydrochloride) (PAH) and anionic titanium(IV) bis (ammonium lactato) dihydroxide (TALH) were deposited onto the bottom electrode using electrostatic LbL assembly. After deposition of the nanocomposite film, thermal annealing and the subsequent deposition of top electrodes on films were performed to complete the device fabrication. The resultant nanocomposite films were composed of TiO_x films containing conductive carbon components (that is, charge trap sites resulting from thermally annealed GO). Although GO sheets as charge trap sites were used in our study, it should be noted that they could be replaced by other charge trap components such as metal nanoparticles. This strategy may be useful for preparing a variety of functional metal oxide films requiring the desired electronic structure or properties as well as resistive switching memory oxide films for RSNM devices.

EXPERIMENTAL PROCEDURE

Preparation of TiO_x films

The concentration of cationic PAH ($M_w = 120\,000$, Alfa Aesar, Jung-gu, Incheon-si, Korea) and anionic TALH (Aldrich, Cheoin-gu, Yongin-si, Gyeonggi-do, Korea) solutions was adjusted to 1 mg ml^{-1} and 50 mg ml^{-1}, respectively. Quartz glasses or Pt-coated Si substrates were given anionic surfaces by irradiation of ultravolet (UV) light. First, these substrates were dipped for 10 min in the PAH solution, washed twice by dipping in water for 1 min and air-dried with a gentle stream of nitrogen. Anionic TALH was

subsequently deposited onto the PAH-coated substrates by using the same adsorption, washing and drying procedures as described above. The resultant multilayer films were thermally annealed at 450 °C for 2 h under nitrogen condition, and additionally annealed at the same temperature for 4 h under oxygen environment.

Preparation of GO-incorporated TiO_x films

The concentration of anionic GO nanosheets with carboxylic acid groups was adjusted to 1 mg ml^{-1}. These GO sheets were electrostatically LbL-assembled with cationic PAH for the preparation of $[(PAH/TALH)_3/(PAH/GO)_1]_5/(PAH/TALH)_3$ multilayer films onto Pt-coated Si substrates. After the multilayer deposition, the formed films were thermally annealed under the same conditions as mentioned above.

Crystal structure and chemical compositions

The crystal structure of LbL-assembled TiO_x films was investigated using X-ray diffraction at room temperature. Data collection was performed in the 2θ range from 25 to 50° using Cu Kα radiation ($\lambda = 1.54$ Å, Model: Bruker D8 Discover (Bruker Corporation, Billerica, MA, USA). X-ray photoelectron spectroscopy (Kratos, Wharfside, Manchester, UK) was performed to determine the binding state of Ti ions and the presence of residual carbons.

UV–Vis spectroscopy

UV–visible (UV–Vis) spectra of multilayers on quartz glass were collected with a Perkin Elmer (Waltham, MA, USA) Lambda 35 UV–Vis spectrometer.

Kelvin force microscopy

Real-space images of charge trap and release states were measured using kelvin force microscopy (KFM) (XE-100, Park Systems, Yeongtong-gu, Suwon-si, Gyeonggi-do, Korea) in contact mode with conducting tips.

Fabrication of resistive switching memory devices

The TiO_x or GO-incorporated films were formed on the Pt-coated Si substrates as described above. The resistive switching memory properties of the resultant nanocomposite films were measured after deposition of Ag electrodes with a 100 μm diameter without any additional thermal treatment. To investigate the resistive switching behavior of LbL multilayered devices, the current–voltage (I–V) curves were measured with a semiconductor parametric analyzer (Agilent 4155B, Agilent Technologies, Santa Clara, CA, USA) in air environment. The pulsed voltage duration dependence of high and low current states was investigated using a semiconductor parametric analyzer (HP 4155A, Hewlett Packard, Palo Alto, CA, USA).

RESULTS AND DISCUSSION

First, the electrostatic LbL assembly of cationic PAH and anionic TALH was performed on quartz substrates for UV–Vis spectroscopy as shown in Figure 1a. A pronounced and broad peak at 250 nm, which corresponds to TALH absorption, is shown in the spectra. The uniform increase in the intensity of the absorbance peak at 250 nm suggests that a regular amount of TALH was deposited per bilayer, indicating PAH/TALH multilayer growth. The inset in Figure 1a shows that the absorbance at 250 nm increases linearly with increasing bilayer number of PAH/TALH. These multilayers could be easily converted to TiO_x nanocomposite films by thermal degradation of organic components when annealed at 450 °C for 6 h (that is, 2 h under nitrogen and then for 4 h under oxygen). Total film thickness of the LbL-assembled multilayers was reduced by up to ~51% of the initial film thickness as confirmed by cross-sectional field-emission scanning electron microscopy (Figure 1b).

The resultant TiO_x nanocomposites showed a strong growth of typical anatase (004) plane peak as confirmed by X-ray diffraction patterns (Figure 2a). Given that conventional TiO_x films prepared from atomic layer deposition have an evident (101) plane peak with a relatively weak (004) plane peak of typical anatase crystals, the structure shown in the LbL-assembled TiO_x films is closely related to the lateral-directed crystalline growth of TALH layers sandwiched between the adjacent PAH layers. Furthermore, the chemical compositions within the LbL-assembled TiO_x films were investigated by X-ray photoelectron spectroscopy (Figure 2b). The thermal annealing process under nitrogen and oxygen induced oxygen deficiencies accompanied by an increase in the local electron concentration. This oxygen-deficient state can be confirmed by the Ti $2p_{3/2}$ peak shifts to a lower binding energy because of the presence of Ti^{3+} ions (that is, oxygen deficiency state). The measured spectrum can be deconvoluted into the two spin-orbit components, which are identified as Ti^{4+} (458.8 eV) and Ti^{3+} (458.3 eV). The Ti^{3+} in the oxygen-deficient state acts as n-type dopants, transforming insulating oxide into semiconducting oxide. Recently, it was reported that an applied electric field could cause the injection of electrons into the conduction band of TiO_2, followed by reduction to metastable Ti^{3+}.[4] This suggests that TiO_x films prepared by LbL assembly can be used as efficient active layers in RSNM devices. On the other hand, in the case of the TiO_x nanocomposite film thermally annealed only under oxygen, the peak intensity ratio of Ti^{3+} to Ti^{4+} ions was significantly increased compared with that of nanocomposite films annealed under nitrogen

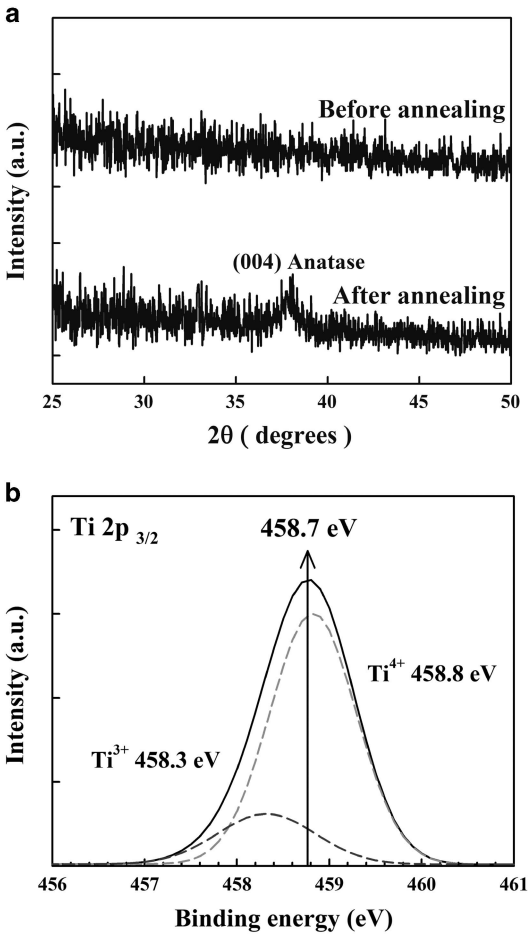

Figure 2 (**a**) X-ray diffraction patterns (XRD) and (**b**) X-ray photoelectron spectroscopy (XPS) of LbL-assembled TiO_x nanocomposite films. LbL, layer-by-layer. A full color version of this figure is available at *Polymer Journal* online.

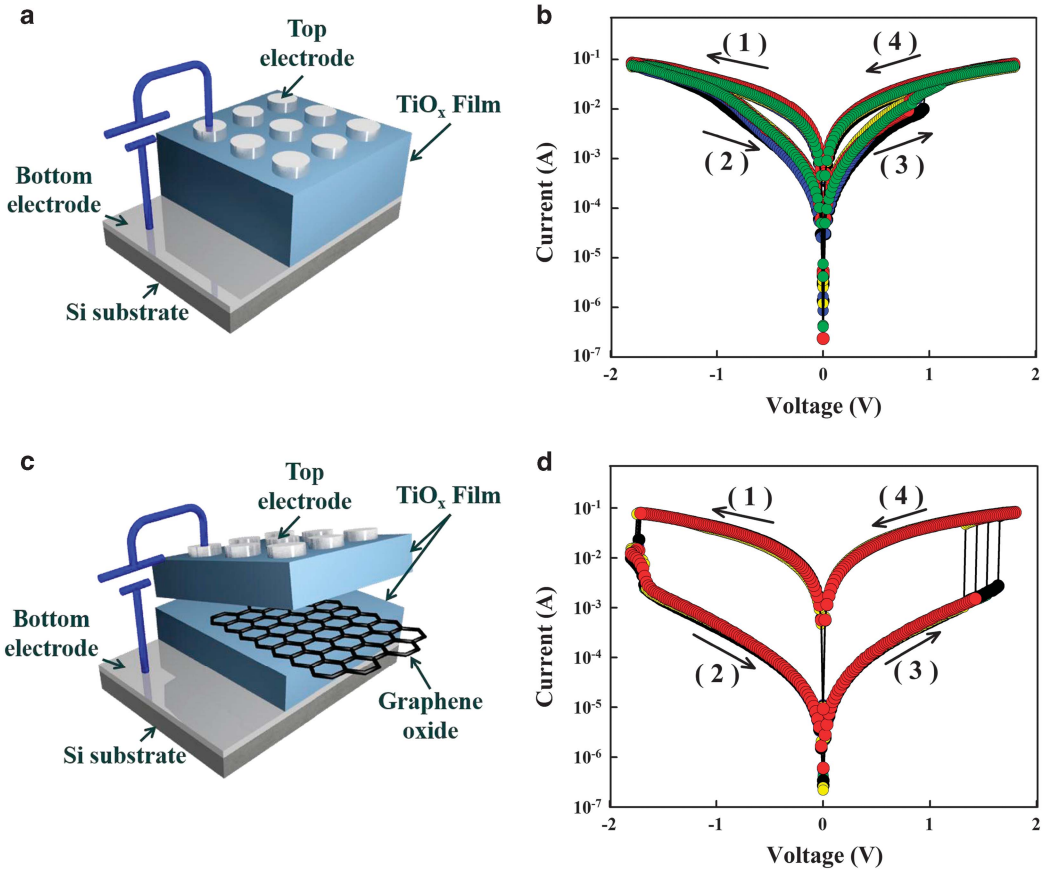

Figure 3 (**a**) Schematic diagram for resistive switching memory devices composed of TiO_x nanocomposite films, $(TiO_x)_{18}$ nanocomposite films. (**b**) *I–V* curves of $(TiO_x\ NC)_{18}$ multilayer device showing repetitive switching cycles after initial electroforming process. (**c**) Schematic diagram for resistive switching memory devices based on GO-incorporated TiO_x nanocomposite films. (**d**) *I–V* curves of thermally annealed $[(PAH/TALH)_3/(PAH/GO)_1]_5/(PAH/TALH)_3$ multilayer device showing bipolar switching behavior.

and oxygen (Supplementary Information, Supplementary Figure S2), and therefore the resultant film was unsuitable for resistive switching memory layer due to the possibility of a high leakage current.

Based on these results, we investigated the resistive switching properties of thermally annealed $(PAH/TALH)_{18}$ multilayers (that is, the $(TiO_x)_{18}$ film with a thickness of 46 ± 2 nm) onto Pt-coated substrates in air condition (Figure 3a). For measurements of typical bipolar switching that depend on the polarity and direction of the applied voltage to form the high and low current states, top Ag electrodes with a diameter of ~100 μm were deposited onto the resulting multilayers, and a voltage sweep from 0 V to −1.8 V and back to +1.8 V was applied after an electroforming process (an initial electric field to generate highly defective components and to create conducting filamentary paths connecting the two electrodes) at ~2.5 V with limited current compliance up to 100 mA. When the voltage polarity applied to the $(TiO_x)_{18}$ nanocomposite devices was reversed, the high current state ('ON' state) that formed after initial electroforming process was converted suddenly to a low current state (RESET process for 'OFF' state) at −1.8 V when the reverse voltage polarity was applied to the nanocomposite film devices (Figure 3b). This low current state ('OFF' state) was maintained from −1.8 V to +1.8 V and converted to the high current state at +1.8 V (SET process for 'ON' state). This electrical bistable property was not observed from the $(TiO_x)_{18}$ film thermally annealed only under oxygen environment (Supplementary Information, Supplementary Figure S3).

Although various switching mechanisms have been proposed for the electrically bistable properties of resistive switching memory devices, the switching behavior shown in our study can be explained by the charge trap model. According to the Simmons–Verderber model,[28] the memory effect with the high and low current states was due to charge storage (high resistance) and release (low resistance) within the charge trap sites. In our system, many material-based defects such as oxygen deficiencies, dislocations, grain boundaries and residual carbons can be used as charge trap sites,[2] which can affect the switching mechanism considerably. When electrons released from charge trap sites during positive voltage sweep from 0 V to −1.8 V (step 1) are trapped in charge trap sites by reversing the voltage polarity (step (1) → (2)), an interior electric field is constructed in the LbL-assembled TiO_x matrix, causing a sudden decrease of electrical conductivity. This transition state corresponds to the RESET process (that is, $V_{RESET} \sim -1$ V). When the voltage polarity is reversed again (step (3) → (4)), the electrons are released from the charge trap sites, which results in an increase in conductivity, corresponding to the SET process (that is, $V_{SET} \sim +1$ V). However, considering that the LbL-assembled $(TiO_x)_{18}$ film devices exhibited a relatively low ON/OFF current ratio of approximately 10^1, we could not exclude the possibility that the charge trap sites within LbL-assembled TiO_x films would be insufficient and resultantly be operated as shallow charge trap sites. That is, when the injected electrons are sufficiently trapped in the charge trap sites by the reverse of voltage polarity, the electrical conductivity can be notably decreased, inducing the high ON/OFF current ratio.

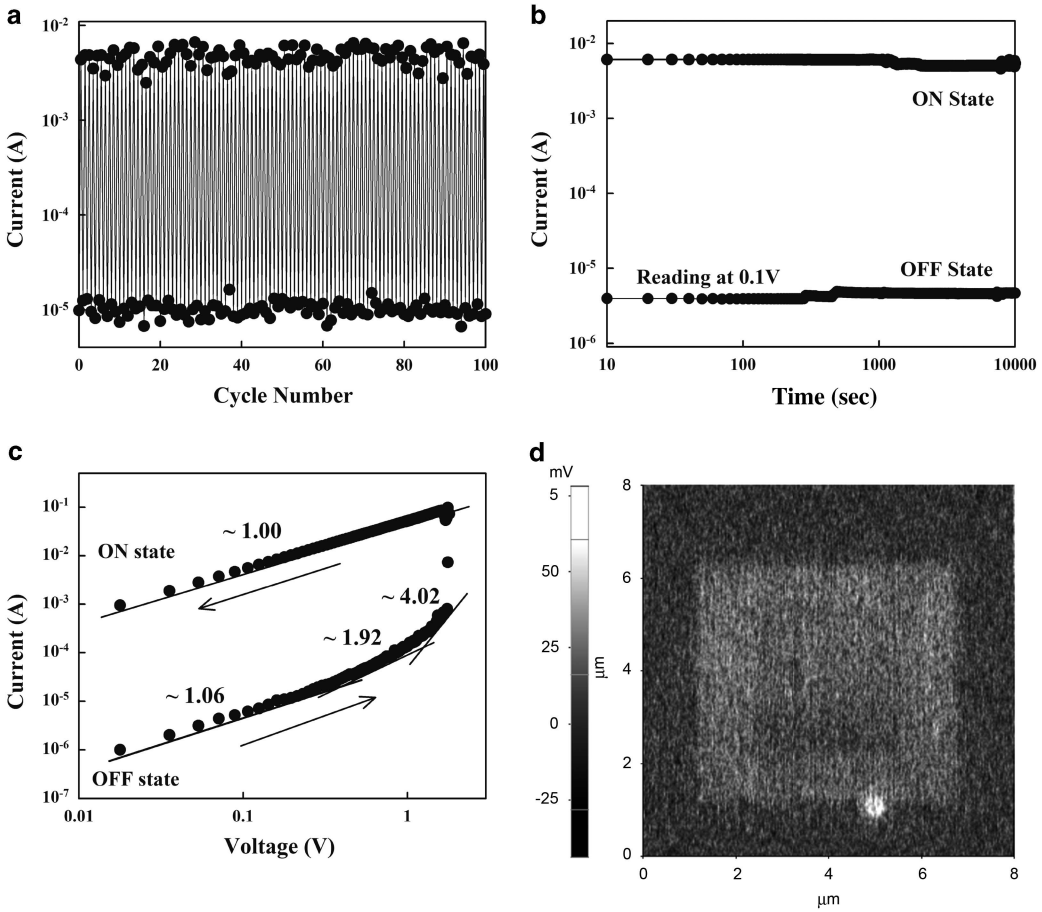

Figure 4 (**a**) Cycling and (**b**) retention time test of GO-incorporated TiO_x multilayer devices. The high and low conductive states were induced using a reading voltage of 0.1 V. The structure of GO-incorporated TiO_x nanocomposite films was identical to that of Figure 3d. (**c**) The linear fitting for the *I–V* curve of GO-incorporated TiO_x devices plotted on a log–log scale during a positive voltage sweep. (**d**) KFM image of GO-incorporated TiO_x nanocomposite films. KFM, kelvin force microscopy. A full color version of this figure is available at *Polymer Journal* online.

To demonstrate these possibilities, the anionic GO sheets containing carboxylic acid moieties were incorporated into the 18 bilayered PAH/TALH multilayers with the aid of cationic PAH, and the formed multilayers (that is, $[(PAH/TALH)_3/(PAH/GO)_1]_5/(PAH/TALH)_3$) were thermally annealed at the same conditions. In this case, the thicknesses of thermally annealed films were increased from 46 ± 2 (without PAH/GO) to 54 ± 3 nm (with five bilayered PAH/GO). Although these film thicknesses could be obtained from single spin-coating of aqueous mixture solution containing GO, TALH and polymer binder such as a poly(vinylpyrrolidone) instead of LbL assembly approach (Supplementary Information, Supplementary Table S1), their surface roughnesses were significantly increased compared with those of LbL-assembled nanocomposite films (Supplementary Information, Supplementary Figure S1). As a result, mixture-blended films were unsuitable for the preparation of TiO_x nanocomposite-based RSNM devices.

Although the GO sheets inserted within TiO_x nanocomposites are thermally decomposed at 450 °C, they can produce a large amount of residual carbons as charge trap sites within TiO_x films. Figure 3c shows the schematic diagram of RSNM devices composed of bottom Pt electrode, $[(PAH/TALH)_3/(PAH/GO)_1]_5/(PAH/TALH)_3$ multilayers and top Ag electrode. Although these GO-incorporated TiO_x devices exhibited the bipolar resistive switching behavior similar to that of $(TiO_x)_{18}$ film device without GO sheets, the ON/OFF current ratio was significantly increased to $\sim 10^3$ (at a reading voltage of +0.1 V) as shown in Figure 3d. These results support the possibilities that the presence of thermally annealed GO can be effectively used as charge trap sites within TiO_x matrices (the more detailed explanation will be shown in the latter part). We also investigated the memory stability of GO-incorporated TiO_x multilayer devices. For this investigation, cycling and retention time tests were performed to determine their electrical stability in the ON and OFF states using a reading voltage of +0.1 V (Figures 4a and b). In this case, it was observed that stable ON and OFF states were maintained during repeated tests of ~100 cycles and a test period of 10^4 s in air. These results show that RSNM devices composed of GO-incorporated TiO_x multilayers exhibit good electrical stability. Furthermore, to understand the conducting behavior of the GO-incorporated TiO_x multilayer devices, the *I–V* characteristics during positive voltage sweep were plotted on a log–log scale (Figure 4c). The *I–V* relationship in the ON state exhibited ohmic conduction behavior with a slope of ~1.00, which indicated the formation of conductive paths in the device during the SET process. In contrast, the conduction behavior in the OFF state followed the trap-controlled space-charge-limited conduction (SCLC) consisting of an ohmic region ($I \propto V^{1.06}$) at a low negative voltage, a transition region ($I \propto V^{1.92}$) from ohmic to SCLC transport and a region of sharp current increase ($I \propto V^{4.02}$).[29]

To further confirm the fact that the switching mechanism of GO-incorporated TiO_x devices is mainly based on the charge trap model, we examined real-space imaging of the charge trap and release state using KFM.[30] The charges stored within thermally annealed GO are detected from the change in the surface potential when the tip of the KFM scans the surface of the GO-incorporated TiO_x layer. First, an $8.0 \times 8.0\ \mu m^2$ area of GO-incorporated TiO_x films was scanned at 9 V for the charge trap state (that is, RESET process). The charge release operation (that is, SET process) was performed by scanning an area of $6.0 \times 6.0\ \mu m^2$ with -9 V applied to the bottom contact. As shown in Figure 4d, the yellow region indicates the charge trap state, and the dark region corresponds to the charge release state. The increased voltage thresholds of the charge trap and release processes may result from an additional energy barrier from interfacial surface contamination on conducting KFM tip surfaces. It is also possible that the KFM tip, because of its small contact area (~50 nm), can operate as an electrical point source, thereby causing the electric field exerted from the tip throughout the nanocomposite films to be non-uniform. A non-uniform electric field is known to increase the applied voltages for resistive switching.[31] However, an obvious fact was that the bipolar switching behavior of GO-incorporated TiO_x devices could be explained by the charge trap mechanism, which was confirmed by the color contrast resulting from the potential difference between the charge trap and charge release states.

CONCLUSIONS

We demonstrated that RSNM devices based on TiO_x nanocomposites could be easily prepared from an electrostatic LbL assembly process, and the insertion of GO nanosheets within TiO_x matrices could significantly improve the ON/OFF current ratio (~10^4). The notable switching property in our system could be explained by the presence of thermally annealed GO sheets operating as charge trap sites, which was confirmed by the changes in real-space imaging of the charge trap and release state using KFM. We also highlight the fact that our approach allows the production of resistive switching-active films with modified electrical properties using the electrostatic LbL assembly.

CONFLICT OF INTEREST

The authors declare no conflict of interest.

ACKNOWLEDGEMENTS

This work was supported by the National Research Foundation (NRF) grant funded by the Ministry of Science, ICT & Future Planning (MSIP) (2015R1A2A1A01004354).

1 Lee, J.-S., Cho, J., Lee, C., Kim, I., Park, J., Kim, Y.-M., Shin, H., Lee, J. & Caruso, F. Layer-by-layer assembled charge trap memory devices with adjustable electronic properties. *Nat. Nanotechnol.* **2**, 790–795 (2007).
2 Waser, R. & Aono, M. Nanoionics-based resistive switching memories. *Nat. Mater.* **6**, 833–840 (2007).
3 Wuttig, M. & Yamada, N. Phase-change materials for rewrittable data storage. *Nat. Mater.* **6**, 824–832 (2007).
4 Yang, J. J., Pickett, M. D., Li, X., Ohlberg, D. A. A., Stewart, D. R. & Williams, R. S. Memristive switching mechanism for metal/oxide/metal nanodevices. *Nat. Nanotechnol.* **3**, 429–433 (2008).
5 Rodríguez Contreras, J., Kohlstedt, H., Poppe, U., Waser, R., Buchal, C. & Pertsev, N. A. Resistive switching in metal-ferroelectric-metal junctions. *Appl. Phys. Lett.* **83**, 4595–4597 (2003).
6 Kinoshita, K., Tamura, T., Aoki, M., Sugiyama, Y. & Tanaka, H. Bias polarity dependent data retention of resistive random access memory consisting of binary transition metal oxide. *Appl. Phys. Lett.* **89**, 103509 (2006).
7 Rohde, C., Choi, B. J., Jeong, D. S., Choi, S., Zhao, J. S. & Hwang, C. S. Identification of a dertermining parameter for resistive switching of TiO_2 thin films. *Appl. Phys. Lett.* **86**, 262907 (2005).
8 Chae, S. C., Lee, J. S., Kim, S., Lee, S. B., Chang, S. H., Liu, C., Kahng, B., Shin, H., Kim, D.-W., Jung, C. U., Seo, S., Lee, M.-J. & Noh, T. W. Random circuit breaker network model for unipolar resistance switching. *Adv. Mater.* **20**, 1154–1159 (2008).
9 Choi, D., Lee, D., Sim, H., Chang, M. & Hwang, H. Reversible resistive switching of $SrTiO_x$ thin films for nonvolatile memory applications. *Appl. Phys. Lett.* **88**, 082904 (2006).
10 Hickmott, T. W. Low-frequency negative resistance in thin anodic oxide films. *J. Appl. Phys.* **33**, 2669–2682 (1962).
11 Zhang, T., Su, Z., Chen, H., Ding, L. & Zhang, W. Resistance switching properties of sol-gel derived $La_{0.67}Ca_{0.33}MnO_3$ thin films on F-doped SnO_2 conducting glass. *Appl. Phys. Lett.* **93**, 172104 (2008).
12 Lin, C.-Y., Lin, C.-C., Huang, C.-H., Lin, C.-H. & Tseng, T.-Y. Resistive switching properties of sol-gel derived Mo-doped $SrZrO_3$ thin films. *Surf. Coat. Technol.* **202**, 1319–1322 (2007).
13 Chang, W.-Y., Cheng, K.-J., Tsai, J.-M., Chen, H.-J., Chen, F., Tsai, M.-J. & Wu, T. B. Improvement of resistive switching characteristics in TiO_2 thin films with embedded Pt nanocrystals. *Appl. Phys. Lett.* **95**, 042104 (2009).
14 Kim, D. C., Seo, S., Ahn, S. E., Suh, D.-S., Lee, M. J., Park, B.-H., Baek, I. G., Kim, H.-J., Yim, E. K., Lee, J. E., Park, S. O., Kim, H. S., Chung, U.-I., Moon, J. T. & Ryu, B. I. Electrical observations of filamentary conductions for the resistive memory switching in NiO films. *Appl. Phys. Lett.* **88**, 202102 (2006).
15 Liu, L. F., Kang, J. F., Xu, N., Sun, X., Chen, C., Sun, B., Wang, Y., Liu, X. Y., Zhang, X. & Han, R. Q. Gd doping improved resistive switching characteristics of TiO_2-based resistive memory devices. *Jpn. J. Appl. Phys.* **47**, 2701 (2008).
16 Guan, W., Long, S., Jia, R. & Liu, M. Nonvolatile resistive switching memory utilizing gold nanocrystals embedded in zirconium oxide. *Appl. Phys. Lett.* **91**, 062111 (2007).
17 Li, G. L., Liu, G., Li, M., Wan, D., Neoh, K. G. & Kang, E. T. Organo- and water-dispersible graphene oxide-polymer nanosheets for organic electronic memory and gold nanocomposites. *J. Phys. Chem. C* **114**, 12742–12748 (2010).
18 Hwang, S. K., Lee, J. M., Kim, S., Park, J. S., Park, H. I., Ahn, C. W., Lee, K. J., Lee, T. & Kim, S. O. Flexible multilevel resistive memory with controlled charge trap B- and N-doped carbon nanotubes. *Nano Lett.* **12**, 2217–2221 (2012).
19 Son, D. I., Park, D. H., Kim, J. B., Choi, J.-W., Kim, T. W., Angadi, B., Yi, Y. & Choi, W. K. Bistable organic memory device with gold nanoparticles embedded in a conducting poly (N-vinylcarbazol) colloids hybrid. *J. Phys. Chem. C* **115**, 2341–2348 (2011).
20 Corbierre, M. K., Cameron, N. S., Sutton, M., Mochrie, S. G., Lurio, L. B., Rühm, A. & Lennox, R. B. Polymer-stabilized gold nanoparticles and their incorporation into polymer matrices. *J. Am. Chem. Soc.* **123**, 10411–10412 (2001).
21 Decher, G. Fuzzy nanoassemblies: toward layered polymeric multicomposites. *Science* **277**, 1232–1237 (1997).
22 Yu, A., Liang, Z., Cho, J. & Caruso, F. Nanostructured electrochemical sensor based on dense gold nanoparticle films. *Nano Lett.* **3**, 1203–1207 (2003).
23 Park, M., Kim, Y., Ko, Y., Cheong, S., Ryu, S. W. & Cho, J. Amphiphilic layer-by-layer assembly overcoming solvent polarity between aqueous and nonpolar media. *J. Am. Chem. Soc.* **136**, 17213–17223 (2014).
24 Cherstvy, A. G. Electrostatics and charge regulation in polyelectrolyte multilayered assembly. *J. Phys. Chem. B* **118**, 4552–4560 (2014).
25 Cho, I., Kim, B. J., Ryu, S. W., Cho, J. H. & Cho, J. Transistor memory devices with large memory windows, using multi-stacking of densely packed, hydrophobic charge trapping metal nanoparticle array. *Nanotechnology* **25**, 505604 (2014).
26 Xiong, Z., Gu, T. & Wang, X. Self-assembled multilayer films of sulfonated graphene and polystyrene-based diazonium salt as photo-crosslinkable supercapacitor electrodes. *Langmuir* **30**, 522–532 (2014).
27 Kim, Y., Zhu, J., Yeom, B., Prima, M. D., Su, X., Kim, J.-G., Yoo, S. J., Uher, C. & Kotov, N. A. Stretchable nanoparticle conductors with self-organized conductive pathways. *Nature* **500**, 59–64 (2013).
28 Simmons, J. G. & Verderber, R. R. New conduction and reversible memory phenomena in thin insulating films. *Proc. R. Soc. A* **301**, 77–102 (1967).
29 Yang, Y. C., Pan, F., Liu, Q., Liu, M. & Zeng, F. Fully room-temperature-fabricated nonvolatile resistive memory for ultrafast and high-density memory application. *Nano Lett.* **9**, 1636–1643 (2009).
30 Ko, Y., Baek, H., Kim, Y., Yoon, M. & Cho, J. Hydrophobic nanoparticle-based nanocomposite films using in situ ligand exchange layer-by-layer assembly and their nonvolatile memory applications. *ACS Nano* **7**, 143–153 (2013).
31 Lee, C., Kim, I., Choi, W., Shin, H. & Cho, J. Resistiveshemistry. *Langmuir* **25**, 4274–4278 (2009).

Supplementary Information accompanies the paper on Polymer Journal website (http://www.nature.com/pj)